Journal of Structural Geology, Vol. 15, No. 8, pp. 1045 to 1054, 1993
Printed in Great Britain

0191-8141/93 $06.00+0.00

Stress inversion methods: are they based on faulty assumptions?

D. D. POLLARD and S. D. SALTZER*

Department of Geology and The Rock Fracture Project, Stanford University, Stanford, CA 94305 U.S.A.

and

ALLAN M. RUBIN

Department of Geological and Geophysical Sciences, Princeton University, Princeton, NJ 08544, U.S.A.

(*Received* 2 *December* 1991; *accepted in revised form* 24 *September* 1992)

Abstract—Stress inversion methods employed by structural geologists for estimating a regional stress tensor from populations of faults containing slickenlines rely on the basic assumption that slip on each fault plane occurs in the direction of maximum resolved regional shear stress. This premise ignores directional differences in fault compliance caused by fault shape, the Earth's surface or frictional anisotropy of the fault itself. It is also assumed that the regional stress field is homogeneous in space and time. Thus, perturbations in the local stress field caused by such things as material heterogeneities near the fault and mechanical interaction with nearby faults are not considered. Regional stresses may exercise dominant control on the slip direction; however local factors may perturb this field. We show how differences in fault compliance and local stress perturbations can result in a measureable difference between the direction of resolved shear stress and the direction of fault slip. Numerical modeling of common fault geometries in an elastic half space provides a means for evaluating the magnitude of this difference. We illustrate a few examples of geological circumstances under which the inversion techniques should be reliable, and a few where errors related to violations of the basic assumptions exceed those inherent to the data gathering and inverse techniques.

INTRODUCTION AND BACKGROUND

ONE of the principal goals of structural geology is to relate observed structures to the causative tectonic forces, thereby illuminating the origin and evolution of the structures and their role in geologic history. In typical 'forward' models the tectonic forces are described in terms of stresses acting at some distance from the locality where the structure might develop (e.g. Hafner 1951, Hubbert 1951, Ode 1957, Couples 1977, Muller & Pollard 1977). In the simplest cases this distance is large compared to the characteristic length of the structure and these 'regional' stresses are assumed to be homogeneous, so they are completely specified by a single stress tensor. Note that the word regional in this context does not imply a particular scale, but rather a relative scale, one that is large compared to the structure. The 'inverse' problem is to deduce the regional stress tensor from an existing geologic structure. For example, several computational methods exist for inferring the components of a regional stress tensor, σ_{ij}^{r}, from populations of faults containing slickenlines (Carey & Brunier 1974, Etchecopar *et al.* 1981, Angelier *et al.* 1982, Gephart & Forsyth 1984, Michael 1984, Reches 1987).

Stress inversion techniques have been applied to fault slickenline data from a variety of tectonic settings and have produced results that are consistent and interpretable. Because of this success, what was until recently a rather esoteric endeavor is now gaining popularity and the gathering of data for this purpose is becoming part of the routine measurements of structural geologists. With few exceptions (Carey-Gailhardis & Mercier 1987, Pershing 1989) the basic assumptions of these techniques have not been evaluated.

To implement the inversion techniques, the maximum resolved regional shear stress direction is equated with the apparent slip direction on each fault. Slip is generally inferred from orientations of frictional grooves or fibrous lineations, termed slickenlines (Fleuty 1974), that are assumed to record the direction of the last increment of slip on a fault surface. Grooves result from the frictional sliding, and fibrous lineations result from alternating increments of opening, due to slip on irregular faults, and mineral precipitation. The long axis of each fiber is parallel to the direction of slip and the sense of imbrication of fibrous sheets corresponds to the sense of motion on the fault (Marshak & Mitra 1988). Field data for each fault includes measurement of fault plane orientation, slip direction, and the sense of slip (Allmendinger 1989).

The analysis of these data is based on the idealization of potential fault planes within a rock mass subject to a homogeneous stress state, σ_{ij}^{r}, referenced to the regional co-ordinate system, x_i^r (Fig. 1). The regional stress tensor, σ_{ij}^{r}, can be transformed to the equivalent stress tensor, σ_{ij}^{f}, referenced to the fault plane co-ordinate system, x_i^f, using the standard tensor transformations (Means 1976):

*Present address: Chevron Oil Field Research Company, P.O. Box 446, La Habra, CA 90633, U.S.A.

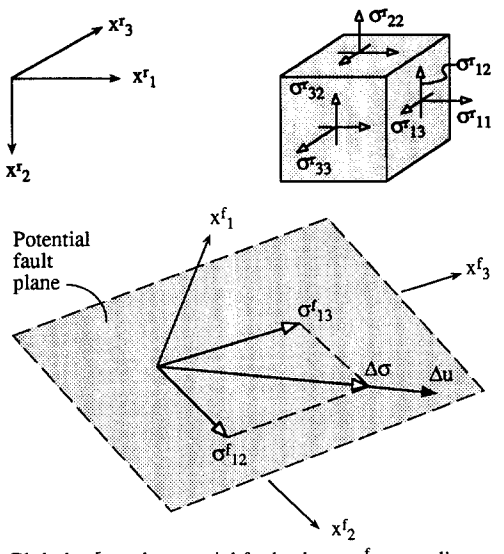

Fig. 1. Global, x_i^r, and potential fault plane, x_i^f, co-ordinate systems; regional stress tensor, σ_{ij}^r, resolved shear stress components, σ_{12}^f and σ_{13}^f, and maximum shear stress, $\Delta\sigma$; displacement discontinuity, Δu.

$$\sigma_{ij}^f = C_{ik}C_{jl}\sigma_{kl}^r, \tag{1}$$

where C_{ik} and C_{jl} are the direction cosines defining the relative orientations of the regional and fault plane co-ordinate systems. For this three-dimensional problem the subscripts i, j, k and l take on values 1, 2 and 3, and repeated subscripts on the right-hand side indicate summation over this range. The superscripts r and f refer to the regional and the fault plane co-ordinate systems. The two shear stress components, σ_{12}^f and σ_{13}^f, acting on the potential fault plane can be resolved vectorially to find the direction of maximum shear stress, $\Delta\sigma$, on this plane before slip. Because the stress field is presumed to be homogeneous, the fault locations, size and shape of the fault periphery are unimportant; only fault orientation plays a role in determining the direction and magnitude of the maximum resolved shear stress.

Next, the assumption is invoked that slip, Δu, will occur in the direction of the maximum resolved shear stress (Fig. 1). It follows that differently-oriented potential faults in the homogeneous regional stress field will slip in different directions depending on their orientation relative to σ_{ij}^r. It also follows that the slip direction will be the same everywhere on a given plane because the resolved shear stress is homogeneous on each plane. In principle, if one knew the maximum resolved shear stress on several differently oriented planes, one could compute the regional stress tensor. In practice, only the orientation, not the magnitude, of the maximum resolved shear stress is inferred from slip directions on individual faults, so only part of the regional stress tensor can be estimated.

The solution procedure that most workers have used involves setting up a system of linear equations based on the assumptions mentioned above for a population of faults, although some authors (Michael 1984, Reches 1987) add additional constraints that are discussed below. This system of equations can be written in matrix form to obtain an equation of the type:

$$A\mathbf{x} = \mathbf{y}, \tag{2}$$

where A is a matrix containing combinations of direction cosines that are related to fault orientations (equation 1), $\mathbf{y}$ is a vector containing shear stress information inferred from slip data for each fault, and $\mathbf{x}$, the vector of unknowns, contains information related to the regional stress tensor. To solve for estimates of the unknown 'model parameters', a least-squares inversion of equation (2) would be (Menke 1984):

$$\mathbf{x} = [A^TA]^{-1}A^T\mathbf{y}. \tag{3}$$

Some workers (Etchecopar *et al.* 1981, Armijo *et al.* 1981, Angelier *et al.* 1982, Gephart & Forsyth 1984) compute a 'reduced stress tensor' composed of three direction cosines defining the orientations of the principal stresses and a ratio of principal stress values, Φ, defined as:

$$\Phi = \frac{(\sigma_2^r - \sigma_3^r)}{(\sigma_1^r - \sigma_3^r)}, \tag{4}$$

where the regional principal stresses are $\sigma_1^r > \sigma_2^r > \sigma_3^r$, so by definition, $0 < \Phi < 1$. These four parameters do not define a unique tensor. To do so, further assumptions must be made about lithostatic stresses or magnitudes of shear stresses (Etchecopar *et al.* 1981).

Following a slightly different approach, Michael (1984) constrains the magnitudes of the shear stress acting across each plane to be equal. Alternatively, Reches (1987) requires that the faults obey the Coulomb yield criterion and slip when the shear stress exceeds frictional resistance to slip. These two authors compute the magnitudes of the regional stress components normalized by the mean stress or the vertical stress. From these values, regional principal stress orientations and normalized magnitudes can be found.

For all of the techniques reviewed above, the computed stress tensor is a model estimate of a homogeneous stress state that is consistent with the observed faulting data, given the basic assumptions. The actual stress state could vary in space over the region of interest and in time over the duration of faulting. Typically, a 'forward' problem specific to the collected data is solved to calculate errors in misfit between the model and the data. For example, Angelier (1979, 1989) and Michael (1984) compare the angular difference between the observed slip directions and the predicted maximum shear stress directions for the model stress state. Gephart & Forsyth (1984) and Gephart (1990) suggest that there is as much uncertainty in fault plane orientations as in slip directions. On the other hand, Reches *et al.* (1992) compute a different solution for each coefficient of friction. They then choose an 'optimum' model that minimizes the sum of the angular difference between the computed regional stress tensor orientation and an 'ideal' stress tensor orientation for each fault.

In summary, the first basic assumption for stress inversion techniques from multiple faults is that the regional stress tensor is spatially and temporally homogeneous throughout the rock mass and over the history

of faulting. We have been careful to refer to the planes used in these techniques as potential fault planes because, once slip occurs, the local stress field will change, and it will be quite heterogeneous (Pollard & Segall 1987). For our evaluation, we take the approach of maintaining a homogeneous remote stress field and allowing local perturbations in the field caused by slip on the faults. The primary focus of this paper is to test the second basic assumption, that the slip on each fault surface has the same direction and sense as the maximum shear stress resolved on each surface from the regional stress field. We suggest that many factors may produce a lack of correspondence between the direction of slip on a fault and the direction of maximum resolved regional shear stress. Below we describe and evaluate three such factors.

EFFECT OF FAULT LENGTH-TO-WIDTH RATIO

The geometry of the periphery of an isolated fault (Fig. 2), which does not approach or intersect other faults or the Earth's surface, can impose a deviation of the slip direction from the maximum resolved shear stress direction because slip is easier in the longer dimension, L, of the fault plane. The periphery is the bounding curve of the two surfaces that make up the fault. These two surfaces are located just to either side of the (x_2^f, x_3^f)-plane at $x_1^f = 0^+$ and $x_1^f = 0^-$. For simplicity we consider only a single slip event which produces a displacement discontinuity between these two surfaces everywhere on a rectangular fault. In general the magnitude of this slip goes to zero at the periphery and varies continuously over the fault.

For large length-to-width ratios, $L/W \gg 1$, faults behave like infinitely-long blade-like cracks and, for this special case, the relationship between slip direction and shear stress direction can be derived analytically for a homogeneous and isotropic elastic body (Pollard & Segall 1987). The regional and fault plane co-ordinate systems are parallel (Fig. 2) and the displacement discontinuity components (slip components) between the two surfaces making up the fault are defined at a particular position, (x_2^f, x_3^f), of the fault as:

$$\Delta u_2 = u_2(x_1^f = 0^+) - u_2(x_1^f = 0^-) \quad (5a)$$

$$\Delta u_3 = u_3(x_1^f = 0^+) - u_3(x_1^f = 0^-). \quad (5b)$$

Here Δu_2 is the slip component parallel to the short dimension, W, and Δu_3 is the slip component parallel to the long dimension, L, for the fault shown in Fig. 2. For a fault with width $W = 2a$, in an elastic body with Poisson's ratio ν, and elastic shear modulus μ, these two components are:

$$\Delta u_2 = \frac{2\Delta\sigma_{12}(1-\nu)}{\mu}[a^2 - (x_2^f)^2]^{1/2} \quad (6a)$$

$$\Delta u_3 = \frac{2\Delta\sigma_{13}}{\mu}[a^2 - (x_2^f)^2]^{1/2}. \quad (6b)$$

Note that the slip components for this two-dimensional fault both vary from maximum values at the center line, $x_2^f = 0$, to zero at the periphery, $x_2^f = \pm a$, but there is no variation along the length of the fault.

The quantities $\Delta\sigma_{12}$ and $\Delta\sigma_{13}$ in equations (6a) and (6b) are the differences between the resolved remote shear stress components on the fault before slip, σ_{12}^r and σ_{13}^r, and the shear stress acting on the fault surfaces after slip, σ_{12}^f and σ_{13}^f:

$$\Delta\sigma_{12} = \sigma_{12}^r - \sigma_{12}^f \quad (7a)$$

$$\Delta\sigma_{13} = \sigma_{13}^r - \sigma_{13}^f. \quad (7b)$$

These differences in shear stress often are referred to as the 'stress drops' during faulting. Unlike the slip components (equations 6a and 6b), the shear stress drop components (equations 7a and 7b) are assumed to be uniformly distributed over the entire fault surface. The uniform stress drop is a prescribed boundary condition for the model and is chosen for simplicity. Nature might provide more complex loading conditions.

The interesting conclusion to be drawn from equations (6a) and (6b) is that, for equal shear stress drops in the two co-ordinate directions ($\Delta\sigma_{12} = \Delta\sigma_{13}$), the blade-like fault slips more in the direction of its length than in its width by the factor $1/(1-\nu)$. We define the *fault compliance* as the ease with which slip occurs in a specific direction on the fault plane. In this simple example, the magnitude of the slip component in the longer direction, Δu_3, is greater than the slip component in the shorter direction, Δu_2, so the fault is more compliant along its length. This result raises the possibility that *the directions of maximum shear stress drop and resolved slip may not coincide on natural faults.*

Although we are concerned primarily with quasi-static elastic displacements, we note here that a

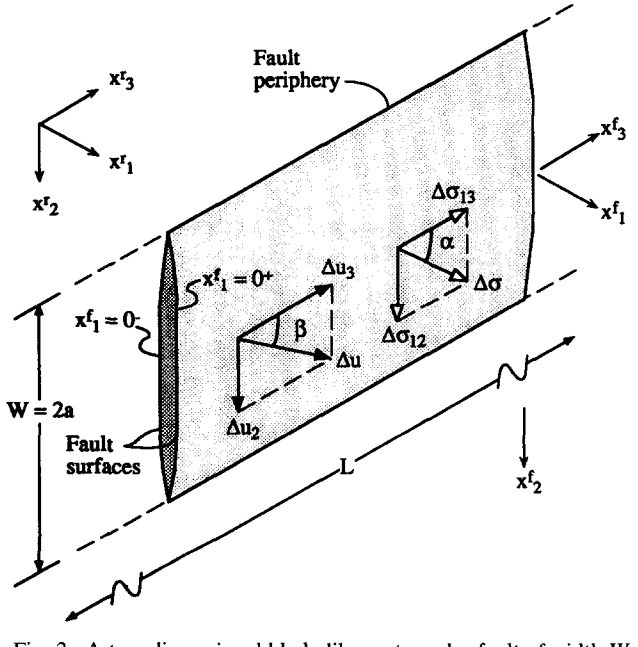

Fig. 2. A two-dimensional blade-like rectangular fault of width $W = 2a$ and length L. Shear stress drop, $\Delta\sigma$, is at angle α to x_3^f and has components, $\Delta\sigma_{12}$ and $\Delta\sigma_{13}$. Displacement discontinuity (slip), Δu, is at angle β to x_3^f and has components, Δu_2 and Δu_3. The two fault surfaces are located at $x_1^f = 0^+$ and $x_1^f = 0^-$, just to either side of the (x_2^f, x_3^f)-plane.

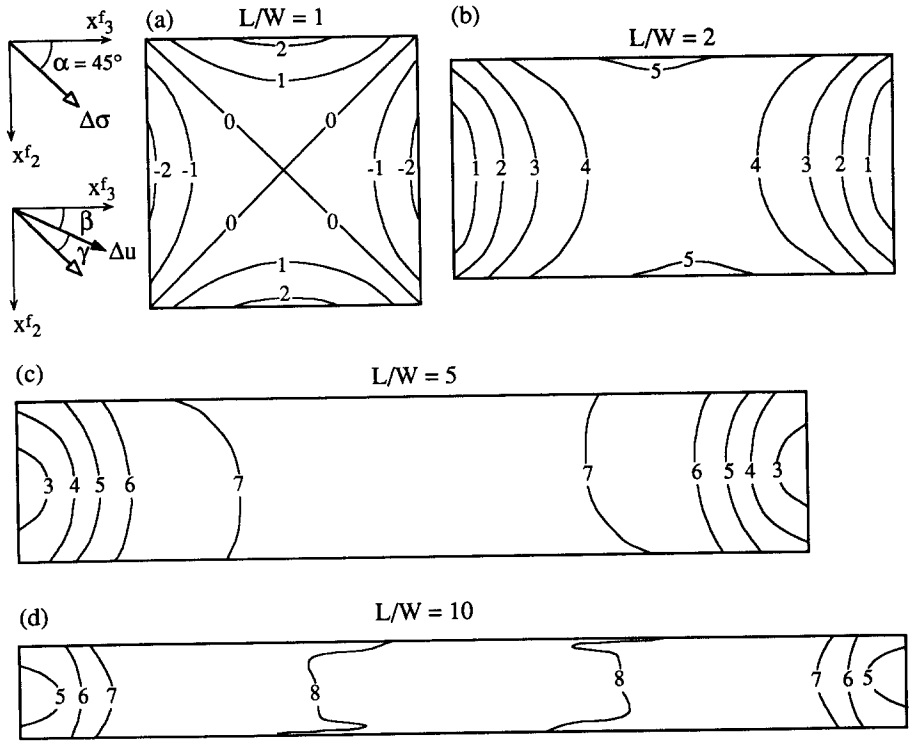

Fig. 3. Contours of the discrepancy angle, γ, on four deeply buried faults of different length-to-width ratios, L/W. Poisson's ratio is $\nu = 0.25$ and the boundary conditions are equal shear stress drop components, $\Delta\sigma_{12} = \Delta\sigma_{13}$. $\gamma = 0$ for a circular fault; compare to (a).

dynamically-propagating fault rupture possesses the same anisotropy of fault compliance as the blade-like fault described above. That is, near the tip of the propagating rupture, shear stresses oriented parallel to the rupture front produce displacements larger, by a factor $1/(1 - \nu)$, than those produced by shear stresses perpendicular to the rupture front (Rice 1980). If earthquakes consist of the passage of a relatively narrow slip 'pulse' (Heaton 1990), then the direction of slickenlines recorded during such an event will be influenced by the anisotropy of fault compliance.

The next step is to quantify the possible angular difference between the directions of maximum shear stress drop and slip. The maximum shear stress drop, $\Delta\sigma$, is oriented at angle α to the x_3^f-direction (Fig. 2), where:

$$\alpha = \tan^{-1}\left[\frac{\Delta\sigma_{12}}{\Delta\sigma_{13}}\right]. \quad (8)$$

The orientation of the slip, Δu, is given by the angle β measured from the x_3^f-direction (Fig. 2), where

$$\beta = \tan^{-1}\left[\frac{\Delta u_2}{\Delta u_3}\right]. \quad (9)$$

The basic assumption of stress inversion techniques can be expressed simply as $\alpha = \beta$.

The angular difference, γ, between the direction of maximum shear stress drop and the direction of slip is defined as:

$$\gamma = \alpha - \beta. \quad (10)$$

For equal shear stress drop components, $\Delta\sigma_{12} = \Delta\sigma_{13}$, equation (8) indicates that $\alpha = 45°$, and substituting equations (6a) and (6b) into equation (9) we find $\beta = \tan^{-1}(1 - \nu)$. Thus, γ for a blade-like fault ($L \gg W$) is given as $\gamma = 45° - \tan^{-1}(1 - \nu)$. For the full range of Poisson's ratios, $0 < \nu < 0.5$, this corresponds to a range of angular discrepancies, $0 < \gamma < 18.43°$.

We have used the computer program DIS3D (Erickson 1987) as modified by Rubin (1992, appendix A) to estimate displacement fields due to slip on a rectangular fault plane in an elastic half space loaded by a homogeneous remote stress field (Fig. 3). Equal shear stress drop components ($\Delta\sigma_{12} = \Delta\sigma_{13}$) are prescribed along a deeply buried fault, so $\alpha = 45°$. Figure 3 illustrates the magnitude of the discrepancy angle, γ, contoured on the fault plane for various length-to-width ratios. Note that the slip magnitude and direction vary over the surface of the fault, with the magnitude falling to zero at the rectangular periphery. Because rectangular faults are more compliant in their longer dimension, we find $\beta < \alpha$, and γ is positive. The distribution of γ does not vary with the size of the fault, but rather with the length-to-width ratio, L/W. Also, these results are independent of the elastic shear modulus, but they do depend upon Poisson's ratio, which is taken as $\nu = 0.25$ for these examples. The largest angular discrepancies for the rectangular faults are found to occur near the fault centers.

Figure 4 is a plot of the discrepancy angle, γ, at the center of the fault plane for length-to-width ratios ranging from 1 to 15. Different curves represent different Poisson's ratios. The magnitude of γ at the fault center for length-to-width ratios exceeding 5:1 ap-

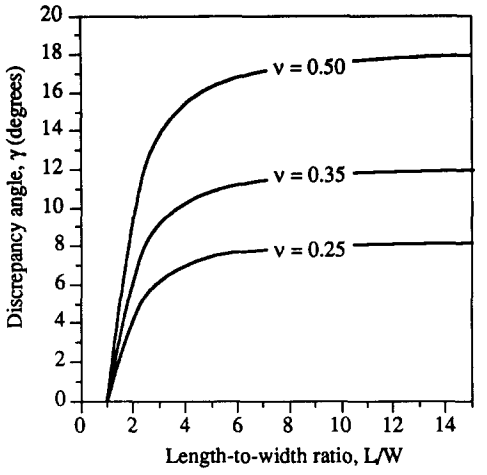

Fig. 4. Contours of discrepancy angle, γ, for rectangular faults with length-to-width ratios from 1 to 15 and three different Poisson's ratios, ν.

proaches (within 1%) the analytical value for infinitely long faults. For values of Poisson's ratio typical of rock, $\nu < 0.35$, the discrepancy angle is less than 12° for all possible length-to-width ratios. Because these discrepancies are not large compared to typical errors introduced during field measurements, or compared to the precision estimated for inversion techniques, we conclude that the effect of length-to-width ratio is not significant.

EFFECT OF THE EARTH'S SURFACE

The boundary conditions on the air–solid interface require the shear and normal tractions to be small (usually taken as zero) compared to stresses within the elastic solid. As a consequence, slip directions on faults located near the Earth's surface will be different from those on a comparable deeply-buried fault. This will affect the magnitude and distribution of the discrepancy angle, γ.

Figures 5(a) & (b) show theoretical contours of γ for two normal faults, dipping at 60° with $L = W$. The boundary conditions are for a pure dip-slip stress drop, so $\Delta\sigma_{13} = 0$ and $\alpha = 90°$. Figure 5(a) shows the distribution of γ on a deeply buried fault plane. The distribution of γ differs from that of Fig. 3(a) where the boundary conditions are equal strike-slip and dip-slip stress drops, so $\alpha = 45°$. Figure 5(b) shows the γ distribution on a 60° dipping normal fault plane which intersects the free surface along its upper periphery. Compare this distribution to that in Fig. 5(a) and note the asymmetry with depth induced by the effect of the free surface.

This example illustrates the fact that proximity of a fault to the surface of the earth at the time of slip can increase the divergence of the slip direction from the direction of maximum shear stress drop. However, values of γ only increase to about ±15°. Furthermore, discrepancies contoured near sharp corners in the periphery, where the fault plane geometry is likely to be unrealistic, probably should be ignored. For this and the few other examples we have investigated, the effect of the Earth's surface is not much greater than field measurement errors or analysis imprecision. We conclude that the effect of the Earth's surface is unlikely to be significant.

EFFECT OF FAULT INTERACTION

If more than one fault is active in a region, the direction of resolved shear stress at a point on a particular fault plane is a function of the regional stress field and the fault orientation, but also of the relative positions and orientations of the other faults, and the slip distributions on those faults. In general the slip direction on a given fault will vary over the fault surface in a complex, but continuous manner. Here we examine two typical cases of fault interaction, but emphasize that there are many other interesting cases that remain to be evaluated.

Extensional steps along strike-slip faults

At right steps along right-lateral faults and left steps along left-lateral faults, slip induces local deformation characterized by lesser mean compressive stresses and extensional strains (Segall & Pollard 1980). A well-known example of two overlapping strike-slip fault segments occurs in the Imperial Valley of California (Fig. 6). Here, the Imperial fault extends southeasterly for at least 60 km and the Brawley fault extends approximately 30 km to the northwest. Mesquite Lake occupies the depression located at the right step between these two right-lateral faults. The 1975 Brawley earthquake swarm consisted of 75 events with $\mathbf{M}_L$ between 3.0 and 4.7 (Johnson & Hadley 1976). The October 15 1979 Imperial Valley earthquake ($\mathbf{M}_L$ = 6.6) ruptured a 30 km segment of the Imperial fault with predominant strike-slip offsets to the southeast and dip-slip offsets near the northwest termination (Sharp *et al.* 1982).

Strike-slip motion on either major fault, due to the regional stress field, causes a perturbation in the local stress field. This perturbation is especially strong near the fault periphery and decays with distance from the fault, becoming negligible at a distance of a few times the fault depth. Here depth is the shortest dimension of these vertical strike-slip faults and is taken to be about 8 km. Therefore, when the Brawley fault slips, the nearby Imperial fault experiences a loading caused by both the regional stress field and the local stresses. The direction of subsequent slip on the Imperial fault will be governed by the combined stress fields.

To ascertain how slip on one strike-slip fault influences the slip distribution on the other, we impose boundary conditions of pure strike-slip stress drop on vertical faults with upper peripheries at the free surface. Figure 7(a) shows values of γ contoured on the model Imperial fault with no slip on the Brawley fault, whereas Fig. 7(b) shows the γ distribution on the model Imperial

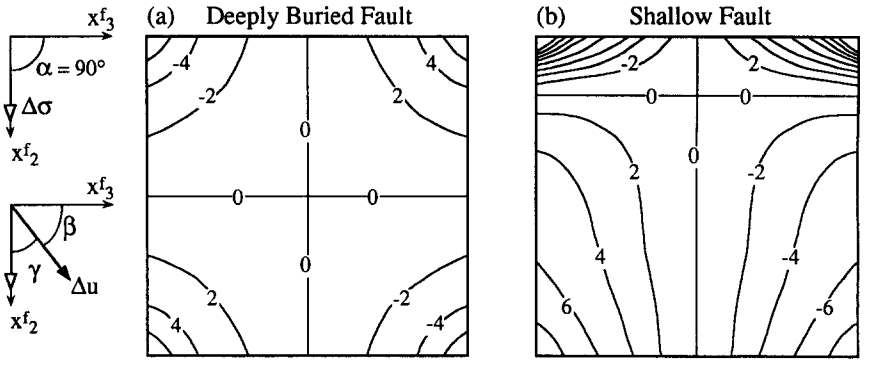

Fig. 5. Contours of discrepancy angle, γ, on deeply buried fault, and on a shallow normal fault dipping 60°.

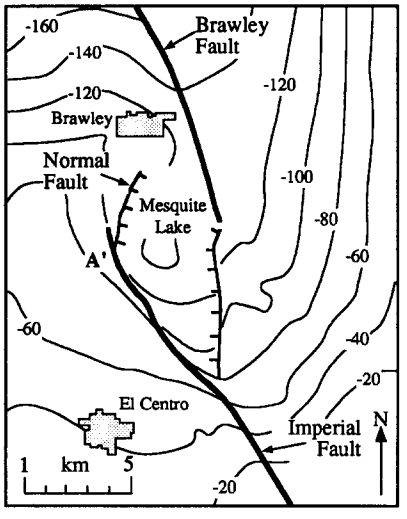

Fig. 6. Map of two overlapping right-lateral right-stepping faults in the Imperial Valley, California (after Johnson & Hadley 1976). Contours of topography in feet.

fault with slip on the Brawley fault. For this geometry, the discrepancy angle is not particularly altered by interaction. Note however, that at depth near the northern end of the Imperial fault (labeled A′ on Figs. 6 and 7), where interaction with the Brawley fault is greatest, γ values are increased by about a factor of two. If the terminations of the two faults were closer together, the discrepancy angles would be greater, but for the geometry of Fig. 6 values of γ are not large enough to jeopardize the stress inversion techniques.

Next consider another common geometry, found in the same area (Fig. 6), consisting of a normal fault striking at 45° to the Imperial fault and extending from its northern termination. The model normal fault dips 60° to the east. For the sake of this example we specify remote boundary conditions consisting of the greatest horizontal compressive stress, S_H, oriented at 45° to the trace of the Imperial fault, the least horizontal compressive stress, S_h, oriented perpendicular to the trace of the normal fault, and the vertical intermediate stress, S_v. Thus, the resolved remote stress acting alone would result in pure strike-slip shear stress on the Imperial fault and pure dip-slip shear stress on the normal fault. However, when interaction is considered the right-lateral motion of the strike-slip fault imparts a considerable right-lateral shear stress on the normal fault.

Figure 8 illustrates the distribution of γ on the Imperial fault and the normal fault. The active segment of the Imperial fault is 16 km long and 8 km deep. The normal fault extends 4 km along strike and 6 km down dip. The value of γ is controlled by the ratio $(S_H - S_h)/(S_v - S_h)$, which in this example was taken to be 2. That is, the vertical stress is the average of the two horizontal principal stresses. Note that the magnitude of γ on the normal fault exceeds 15° over about 75% of the fault and reaches a maximum of about 25°.

The magnitude of γ on the normal fault increases as the length of the strike-slip fault increases. The angular discrepancy also increases as S_H rotates toward the strike of the Imperial fault, so the remote resolved shear stress on the normal fault becomes left-lateral. The magnitude of γ also increases as the stress ratio $(S_H - S_h)/(S_v - S_h)$ increases. If fault friction is introduced, then the stress drop on the strike-slip fault $\Delta\sigma_{13}$ is less than $0.5(S_H - S_h)$, and the relevant stress ratio that controls the magnitude of γ becomes $\Delta\sigma_{13}/[0.5(S_v - S_h)]$. This means that S_v must be closer to S_h than to S_H in order to produce the same values of γ shown in Fig. 8.

Although the sensitivity of γ to the various parameters in these models has not been explored fully, it is clear that the slip direction along small faults near the ends of larger faults can deviate significantly from the direction of resolved shear stress due to the remote loads. For fault geometries such as this, the basic assumption of the stress inversion techniques is not valid.

Conjugate faults

Conjugate faults have been described at scales ranging from outcrop to crustal and often are interpreted as forming in one episode of deformation with a constant regional stress field. In rare instances the relative ages of slip have been documented, verifying that members of two sets of faults were active in an alternating sequence (Zhao & Johnson 1991). For conjugate faults that are widely spaced relative to their lengths the effect of fault interaction will be weak, so slip direction is controlled by the regional stress field. However, for closely-spaced conjugate faults, interaction may be significant. Here we describe an example of the effect of mechanical interaction of conjugate faults on the discrepancy angle, γ, as it depends on the spatial density of the faults.

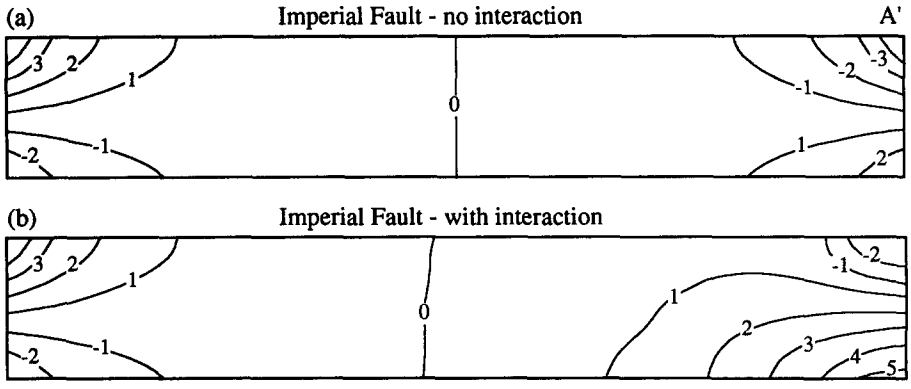

Fig. 7. Contours of discrepancy angle, γ, on a model of a section of the Imperial fault. (a) No interaction with the Brawley fault. (b) Including interaction with the Brawley fault.

Figure 9(a) shows the model consisting of four faults, each perpendicular to the (x_1^r, x_3^r)-plane and oriented at $+30°$ or $-30°$ to the x_1^r-direction. The scale bar indicates the uniform fault depth in the x_2^r-direction. The (x_1^r, x_3^r)-plane is taken as a traction-free surface, so this model can be thought of as a set of vertical, strike-slip faults. We impose a remote uniaxial compressive stress, $-\sigma_{11}^r$, in the x_1^r-direction and set all other remote stresses to zero. This boundary condition results in a maximum resolved shear stress which acts in the (x_1^r, x_3^r)-plane on each fault plane.

The left-lateral fault labeled A–A′ is singled out and contours of γ on the fault plane are illustrated in Fig. 9(b). The maximum resolved regional shear stress acts in the x_3^f-direction on this fault plane so $\alpha = 0°$ and $\gamma = -\beta$. The pattern of γ contours is very similar to that in Fig. 5(a) if rotated 90° to account for the different direction of shear stress. The slight asymmetry of contours in the x_2^f-direction is due to the free surface effect, and the asymmetry in the x_3^f-direction is due to minor interaction with neighboring faults. The magnitude of γ increases toward the corners of the fault periphery to a maximum of about 12°.

A histogram of discrepancy angles, γ, over all four faults of Fig. 9(a) is shown in Fig. 10(a). This histogram was constructed by computing γ at 81 uniformly distributed locations (not including fault peripheries) on each of the four faults. The 324 values of γ were grouped into 1° classes, the number of values in each class is calculated, and these numbers are plotted on the histogram. The distributions of γ values is nearly symmetrical and centered with a strong peak at 0°. The maximum discrepancies are ±11°. We conclude that mechanical interaction does not play a significant role in changing the values of γ for the low spatial density of conjugate faults chosen for this example.

Our second example consists of 11 faults, the original four faults and seven additional faults, in a region of the same size (Fig. 11a), so the faults have a higher spatial density than those in Fig. 9(a). The same remote stress boundary condition is applied and contours of γ on the left-lateral fault A–A′ are illustrated in Fig. 9(b). The lack of symmetry in any direction on the fault plane is indicative of significant mechanical interaction with neighboring faults. Values of γ range from a minimum of about $-35°$ to a maximum of about $+10°$.

A histogram of descrepancy angles (Fig. 10b) was constructed by computing γ at 36 uniformly distributed locations on each of the 11 faults for a total of 396 values. The distribution of γ on the histogram ranges from $-40°$ to $+26°$ and the peak values are centered to the positive side of 0°. These results illustrate that a higher spatial density of faults can enhance mechanical interaction and alter slip directions. In some cases the slip directions are significantly different (>15°) from the direction of resolved regional shear stress, and points with these large angular discrepancies are not necessarily located near sharp corners of fault peripheries.

The stress inversion techniques discussed in the section Introduction and Background do not consider local stress perturbations caused by nearby faults. This conjugate fault example shows how one of the basic assumptions of stress inversion techniques may be violated and casts some doubt on the ability of these techniques to

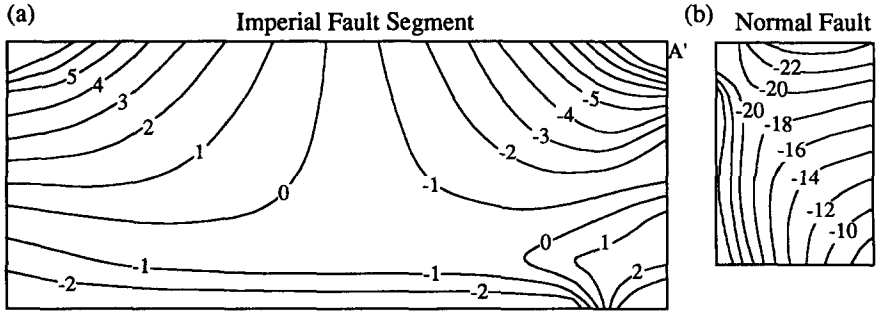

Fig. 8. Contours of discrepancy angle, γ, on a model of a segment of the Imperial fault and on the adjacent normal fault. Mechanical interaction is included.

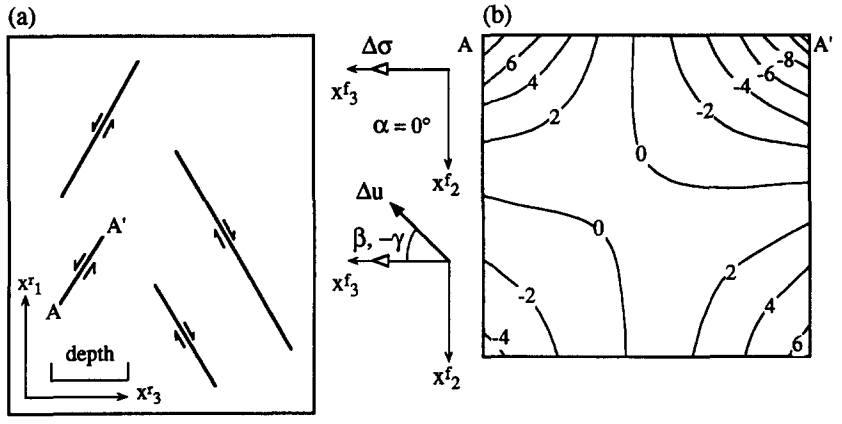

Fig. 9. Model conjugate faults of low spatial density. (a) Geometry of four conjugate faults in map view. (b) Contours of discrepancy angle, γ, on fault A–A′ due to interaction with free surface and with neighboring faults.

predict stress tensors correctly in regions of high fault densities.

CONCLUSIONS

Our analysis suggests that slip directions on certain faults will be controlled primarily by a homogeneous regional state of stress and the orientation of the fault plane. In these cases the basic assumptions of stress inversion techniques are valid. On the other hand, we have shown that slip directions on other faults can be strongly influenced by local factors, such as fault interaction. In these cases the basic assumptions of the inversion techniques are open to question.

The simple examples used here are meant to illustrate the concept that the direction of shear stress drop and slip do not always coincide on a fault plane, and also that a homogeneous stress field may be a poor approximation in the vicinity of a fault. For models of single rectangular faults that we have examined, the slip directions deviated by less than 20° from the direction of stress drop. Over most of the fault surface the angular discrepancies are less than 10°. These angles are within the precision of many field data measurements and stress inversion analyses (e.g. Gephart & Forsyth 1984).

On the other hand, the example of a normal fault near the termination of a larger strike-slip fault demonstrates that discrepancy angles can be significant where faults interact. The stress inversion techniques are usually applied to a population of many faults. Our example involving a population of mechanically interacting conjugate faults illustrates the potential for some fault geometries and spatial densities to result in large discrepancies (up to 40° in this case) between shear stress drop and slip directions. Such discrepancies may adversely affect the stress tensors computed by the inversion techniques.

To test this assertion, we are designing a set of numerical experiments in which synthetic data on slip directions, generated for sets of model faults using DIS3D, are used as input for one or more of the stress inversion programs. The regional stress tensor estimated by inversion could then be compared to the known stress tensor used as the boundary condition for the model. These studies should provide a more complete evaluation of the inversion techniques for dense arrays of natural faults.

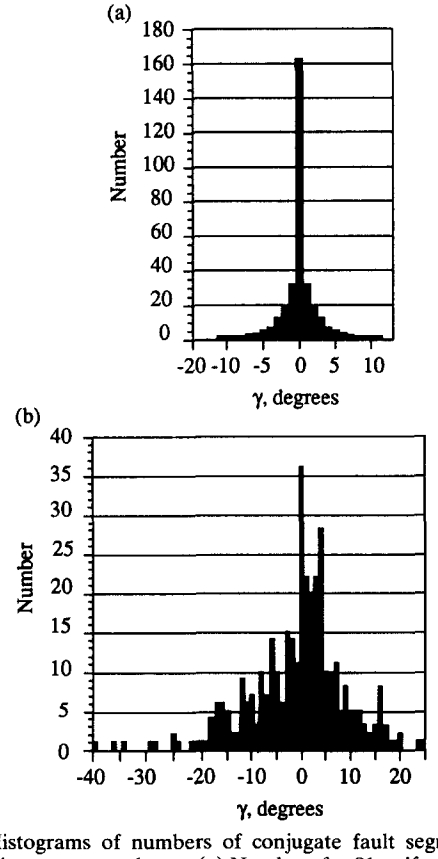

Fig. 10. Histograms of numbers of conjugate fault segments with common discrepancy angles, γ. (a) Numbers for 81 uniformly-spaced locations on each of the four fault planes in Fig. 9. (b) Numbers for 36 uniformly-spaced locations on each of 11 fault planes in Fig. 11.

Acknowledgements—This work was supported by a grant from the United States National Science Foundation (grant EAR-9017909). The authors would like to thank J. L. Mercier, R. W. Allmendinger and J. Gephart for thoughful and constructive reviews of their results. D. D. Pollard thanks R. W. Allmendinger for stimulating his interest in the subject of stress inversion from fault data.

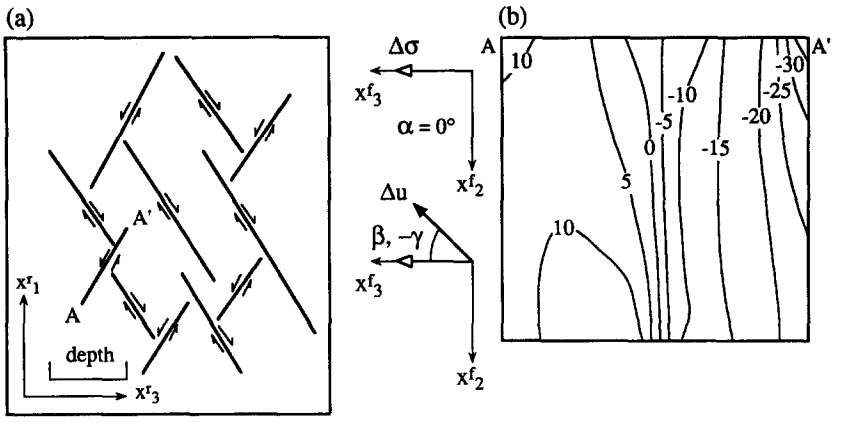

Fig. 11. Model conjugate faults of high spatial density. (a) Geometry of 11 conjugate faults in map view. (b) Contours of discrepancy angle, γ, on fault A–A' due to interaction with free surface and with neighboring faults.

REFERENCES

Allmendinger, R. W. 1989. Notes on fault slip analysis, In: *Quantitative Interpretation of Joints and Faults*. GSA Short Course Manual, GSA Annual Meeting, St. Louis, 1–68.

Angelier, J. 1979. Determination of the mean principal directions of stresses for a given fault population. *Tectonophysics* **56**, T17–T26.

Angelier, J. 1989. From orientation to magnitudes in paleostress determination using fault slip data. *J. Struct. Geol.* **11**, 37–50.

Angelier, J. Tarantola, A., Valette, B. & Manoussis, S. 1982. Inversion of field data in fault tectonics to obtain the regional stress—1. Single phase fault populations: a new method of computing the stress tensor. *Geophys. J. R. astr. Soc.* **69**, 607–621.

Armijo, R., Carey, E. & Cisternal, A. 1982. The inverse problem in microtectonics and the separation of tectonic phases. *Tectonophysics* **82**, 145–160.

Carey, E. & Brunier, B. 1974. Analyse théorique et numérique d'un modèle méchanique élémentaire appliqué a l'étude d'une population de failles. *C.r. Acad. Sci., Paris, Ser. D* **279**, 891–894.

Carey-Gailhardis, E. & Mercier, J. L. 1987. A numerical method for determining the state of stress using focal mechanisms of earthquake populations: application to Tibetan teleseisms and microseismicity of southern Peru. *Earth Planet. Sci. Lett.* **82**, 165–179.

Converse, G. 1973. Equations for the displacements and displacement derivatives due to a rectangular dislocation in a three-dimensional elastic half-space. Unpublished U.S. Geological Survey Report, Menlo Park.

Couples, G. 1977. Stress and shear fracture (fault) patterns resulting from a suite of complicated boundary conditions with applications to the Wind River Mountains. *Pure & Appl. Geophys.* **115**, 113–133.

Crouch, S. L. 1979. Computer simulation of mining in faulted ground. *J. S. Afr. Inst. Min. Metall.* **79**, 159–173.

Crouch, S. L. & Starfield, A. M. 1983. *Boundary Element Methods in Solid Mechanics*. George Allen & Unwin, London.

Erickson, L. 1987. User's manual for DIS3D: A three-dimensional dislocation program with applications to faulting in the Earth. Unpublished M.S. thesis, Standford University, Stanford, California.

Etchecopar, A., Vasseur, G. & Daignieres, M. 1981. An inverse problem in microtectonics for the determination of stress tensors from fault striation analysis. *J. Struct. Geol.* **3**, 51–65.

Fleuty, M. J. 1974. Slickensides and slickenlines. *Geol. Mag.* **112**, 319–322.

Gephart, J. W. & Forsyth, D. W. 1984. An improved method for determining the regional stress tensor using earthquake focal mechanism data: Application to the San Fernando earthquake sequence. *J. geophys. Res.* **89**, 9305–9320.

Gephart, J. W. 1990. Stress and the direction of slip on fault planes. *Tectonophysics* **8**, 845–858.

Hafner, W. 1951. Stress distributions and faulting. *Bull. geol. Soc. Am.* **62**, 373–398.

Heaton, T. H. 1990. Evidence for and implications of self-healing pulses of slip in earthquake rupture. *Phys. Earth & Planet. Interiors* **64**, 1–20.

Hubbert, M. K. 1951. Mechanical basis for certain familiar geologic structures. *Bull. geol. Soc. Am.* **62**, 355–372.

Johnson, C. E. & Hadley, D. M. 1976. Tectonic implications of the Brawley earthquake swarm, Imperial Valley, California, January 1975. *Bull. seism. Soc. Am.* **66**, 1133–1144.

Marshak, S. & Mitra, G. 1988. *Basic Methods of Structural Geology*. Prentice-Hall, Englewood Cliffs, New Jersey.

Means, W. D. 1976. *Stress and Strain*. Springer, New York.

Menke, W. 1984. *Geophysical Data Analysis: Discrete Inverse Theory*. Academic Press, Orlando, Florida.

Michael, A. J. 1984. Determination of stress from slip data: faults and folds. *J. geophys. Res.* **89**, 11,517–11,526.

Muller, O. H. & Pollard, D. D. 1977. The stress state near Spanish Peaks, Colorado determined from a dike pattern. *Pure & Appl. Geophys.* **115**, 69–86.

Ode, H. 1957. Mechanical analysis of the dike pattern of the Spanish Peaks area, Colorado. *Bull. geol. Soc. Am.* **68**, 567–576.

Pershing, J. C. 1989. Modeling discontinuum rock mass behavior: a test of paleostress analyses. *Geol. Soc. Am. Abs. w. Prog.* **21**, A265.

Pollard, D. D. & Segall, P. 1987. Theoretical displacements and stresses near fractures in rock: with applications to faults, joints, veins, dikes, and solution surfaces. In: *Fracture Mechanics of Rock* (edited by Atkinson, B. K.). Academic Press, London.

Reches, Z. 1987. Determination of the tectonic stress tensor from slip along faults that obey the Coulomb yield condition. *Tectonics* **6**, 849–861.

Reches Z., Baer, G. & Hatzor, Y. 1992. Constraints on the strength of the upper crust from stress inversion of fault slip data. *J. geophys. Res.* **97**, 12,481–12,493.

Rice, J. R. 1980. The mechanics of earthquake rupture. In: *Physics of the Earth's Interior* (edited by Dziewonski, A. M. & Boschi, E.). *Proc. Int. School Phys. Enrico Fermi* **78**, 555–649.

Rubin, A. M. 1992. Dike-induced faulting and graben subsidence in volcanic rift zones. *J. geophys. Res.* **97**, 1839–1858.

Segall, P. & Pollard D. D. 1980. Mechanics of discontinuous faulting. *J. geophys. Res.* **85**, 4337–4350.

Sharp, R. V., *et al.* 1982. Surface faulting in the Central Imperial valley. In: *The Imperial Valley, California, Earthquake of October* 15 1979. *Prof. Pap. U.S. geol. Surv.* **1254**, 119–143.

Volterra, V. 1907. Sur l'equibre des corps elastiques multiplement connexes. *Annls scient. Écl. Norm. sup., Paris* **3**, 401–517.

Zhao, G. & Johnson, A. M. 1991. Sequential and incremental formation of conjugate sets of faults. *J. Struct. Geol.* **13**, 887–895.

APPENDIX

We have used the program DIS3D (Erickson 1987) to compute the angular discrepancy between the slip direction and the resolved shear stress along faults. The program is based on analytic solutions for the static elastic stress and displacement fields due to a uniform step discontinuity in displacement across rectangular faults in an elastic half-space (Converse 1973). This solution was found using the point force solutions of Volterra (1907). The program was modified by Rubin (1992) to approximate numerically the case of a prescribed stress boundary condition along a single or several interacting faults, using a boundary-element method similar to that described for two dimensions (Crouch 1979, Crouch & Starfield 1983).

The faults are embedded within a region subjected to a uniform remote stress field, and either a stress boundary condition or a coefficient of friction is specified for each fault plane. Each fault is then subdivided into a grid of rectangular subfaults, and uniform displacements are applied to the subfaults such that the shear stress at the center of each is equal either to the prescribed stress or to the coefficient of friction times the normal stress. By subdividing the faults into finer and finer grids, the numerical solution can be made increasingly accurate. The slip direction of each subfault can then be compared to the direction of resolved remote shear stress on the fault plane to calculate the discrepancy angle.

Fault slip can influence the slip direction of neighboring faults (or neighboring regions of the same fault) directly, by perturbing the shear stress on those surfaces, or indirectly, by changing the normal stress acting across those surfaces. Changing the normal stress results in a change in slip magnitude through the influence of the coefficient of friction, and this may lead to changes in fault interaction and hence slip direction. In the examples cited in this paper, the coefficient of friction has been set to zero. This is equivalent to examining changes in slip direction that result only from the shear stress perturbation due to fault slip.

The original computer program DIS3D (in FORTRAN for UNIX operating systems) and a users manual are available by writing to D. D. Pollard, Geology Department, Stanford University, Stanford, CA 94305, U.S.A. A modest fee will be charged for mailing, printing and media costs.